DESIGN OF A HIGH SPEED ROTATING LOSS TEST RIG FOR RADIAL MAGNETIC BEARINGS

Mary E. F. Kasarda
Paul E. Allaire
Eric H. Maslen
George T. Gillies
University of Virginia, Charlottesville, VA, USA

Nomenclature

B_{max} = maximum magnetic flux density
C_e = eddy current coefficient
C_{ha} = alternating hysteresis coefficient
C_{hr} = rotational hysteresis coefficient
D = diameter of journal
f = rotational frequency
f' = frequency component
g = gap length
i_b = bias current
J = rotor moment of inertia
k = hysteresis empirical exponent
L = length of journal
M_e = eddy current frequency factor
M_v = effective volume factor
M_w = windage loss pole factor
P_e = eddy current power loss
P_{ha} = alternating hysteresis power loss
P_{hr} = rotating hysteresis power loss
R = rotor lamination radius
t = time
ρ = resistivity
ρ_g = density of gas (air)
η = hysteresis empirical coefficient
υ = viscosity of gas (air)
ω = rotor angular velocity
μ = static permeability
τ = lamination thickness
V = volume

ABSTRACT

This paper describes the design and operating characteristics of a vacuum rundown test rig for the measurement of rotating losses in radial magnetic bearings. These rotating losses are due to eddy currents, alternating hysteresis, rotating hysteresis, and windage which create drag on a rotating shaft. The rig consists of a shaft supported in two radial magnetic bearings. The shaft is accelerated by end-mounted electric motors, whose stators can be withdrawn from the shaft after run-up to eliminate any residual magnetic coupling, at which point coast down times due only to drag from the magnetic bearings will be measured. Temperature rises will also be monitored. Different levels of vacuum can be employed to quantify the windage losses. Losses will be measured in several different bearing configurations, both radial planar and homopolar, and the individual loss mechanisms identified and quantified wherever possible. The experimental results will be compared with theoretical models of loss mechanisms. An accurate characterization of the loss mechanisms will aid in calculations of losses and temperature rise in future applications.

INTRODUCTION

Power losses in the magnetic bearings of rotating machinery can create undesired levels of heating and can result in the reduction of machine efficiency. Therefore, the characterization of power loss in bearings is a critical task for the designer of rotating equipment. The increased use of magnetic bearings in various capacities, including high speed aerospace applications, dictates the need to quantify power losses in this type of bearing. While some work has been done to analytically predict losses in magnetic bearings, the authors are unaware of any analytical predictions for high speed losses in large-scale magnetic bearing rotors which have been verified experimentally. The goal of the present study is to develop general power loss equations for high speed operation of magnetic bearings and then to verify them experimentally. In this paper, we describe the test

apparatus which will be used to measure the losses and then briefly describe the expected phenomena associated with magnetic bearing operation at high speeds, detailing the parameters expected to have the greatest impact on power loss.

BACKGROUND

Several researchers in recent years have attempted to quantify the power losses in magnetic bearings. Yoshima [1] discussed an eddy current effect using a detailed finite element model to calculate the magnetic flux in the bearing. The effect of the magnetic force from the induced eddy currents was discussed but losses were not quantified. Matsumura et al. [2] presented a Fourier analysis of the distribution of the magnetic field for an alternating pole (NSNS) and a paired pole (NNSS) arrangement. The paper gave a theoretical prediction of higher losses in the alternating pole arrangement. Experimental results show only a slight difference in the losses at lower speeds with identical losses at higher speeds. Higuchi et al.[3], gave short reports on experimental studies of rotating losses in magnetic bearings. Ueyama and Fujimoto [4] evaluated power losses in a test rig with a magnetic bearing-supported spindle. Iron and windage loss effects were studied for an eight-pole radial magnetic bearing of conventional design. Deceleration studies gave the iron losses for four materials when the chamber was placed in a vacuum. Hysteresis and eddy current coefficients were determined from the experimental results, but no comparison to theoretical predictions was made.

Controversy over rotor losses for various bearing geometries during high speed operation persists because of the absence of a comprehensive study of losses. The purpose of this investigation is to quantify such losses in various bearing configurations and to develop analytical expressions to accurately predict the losses in the design phase of future magnetic bearings. Preliminary work by Kasarda et al.[5] presented a comparison between analytical loss models and experimental results for low speed run-down tests in air up to a DN of about 175,000. DN is calculated by multiplying the diameter of the journal (mm) by the rotational speed (rpm). The analytical model characterized the overall power loss to be the result of four separate mechanisms: alternating hysteresis, rotational hysteresis, eddy current damping, and windage, with certain assumptions. The analytical expression for the alternating hysteresis is [6]

$$P_{ha} = 10^{-7} \eta f' B_{\max}^{k} V \qquad (1)$$

The analytical expression for rotational hysteresis power loss in silicon-iron at low bias flux is [7]

$$P_{hr} = 3.60x10^{-5} f' V \qquad (2)$$

The analytical expression for eddy current losses at low speeds is [8]

$$P_e = \frac{10^{-16} \pi^2 \tau^2 B_{\max}^2 f'^2 V}{6\rho} \qquad (3)$$

These equations were expanded for application to magnetic bearings from classical equations which were developed for non rotating devices such as transformers as well as rotating machines such as electric motors. The important frequency component (f') is different for each magnetic phenomenon (alternating hysteresis, rotational hysteresis, and eddy currents) when applied to magnetic bearings. Note that the eddy current formula in (3) increases as the square of frequency whereas the two hysteresis component formulas (1) and (2) increase linearly with frequency. These frequency relationships will be instrumental in the separation of the loss components. Based upon a boundary layer calculation, the analytical expression for windage losses is [9]

$$P_w = .074 \rho_g L \pi R^4 \omega^3 \left(\frac{\upsilon}{2\pi R^2 \omega} \right)^{0.2} \qquad (4)$$

The overall discrepancy between measured and calculated power losses was ≤ 24% for all of the test configurations [5]. An example of the measured and calculated values is shown in Figure 1. While these low speed tests showed good agreement between measured and calculated values, they are not expected to be adequate for characterizing losses at higher speeds. However, these preliminary analytical loss models represent the foundation for the more comprehensive high speed tests to be run with the test set-up described in the next section.

TEST SET-UP

The new test rotor is designed to run up to a maximum DN of about 4.5 $x10^6$ as illustrated conceptually in Figure 2. The rotor consists of a shaft with two magnetic bearings and two induction motor rotors located at the shaft ends as shown in Figure 2.

The test rig is designed to simplify the variation of parameters including magnetic bearing stator geometry, journal material, lamination thickness, and gap length. The test rig has been designed to measure the power losses in magnetic bearings by accurately measuring the conversion of the rotor's kinetic energy into heat. This is done simply by measuring the time it takes for the rotor to run down from one given speed to another. The kinetic energy of the rotor due to rotation is

$$E_k = \frac{1}{2} J \omega^2 \qquad (5)$$

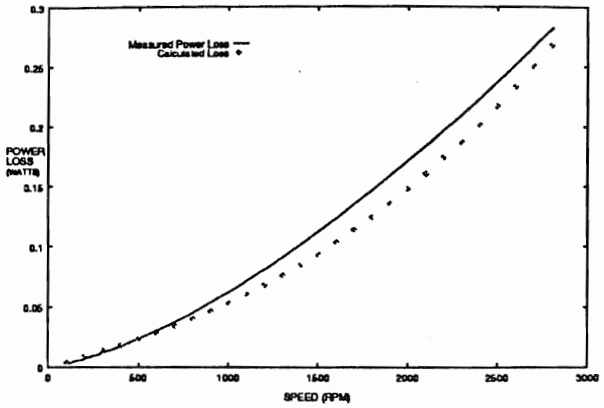

FIGURE 1: Measured and Calculated Power Loss vs. Speed, Ib=1.6, Paired Poles

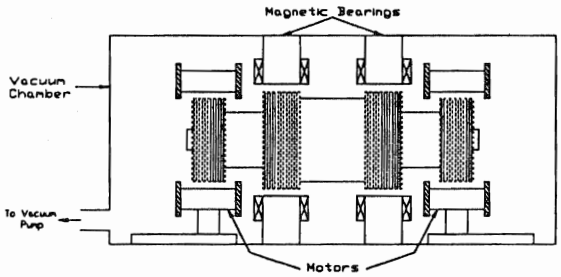

FIGURE 2: Test Set-up: Runup

This kinetic energy is converted to heat in the journal laminations as the rotor decelerates. The power loss is the time derivative of the kinetic energy

$$P_k = \frac{dE_k}{dt} = \frac{d}{dt}\left(\frac{1}{2}J\omega^2\right) = J\omega\frac{d\omega}{dt} + \frac{\omega^2}{2}\frac{dJ}{dt} \qquad (6)$$

If the rotor materials do not have large dimensional changes as their temperature increases, the second term in Equation (6) is negligible. Values for the rotor polar moment of inertia (J) are easily calculated and $\omega(t)$ is measured so P_k is determined. The test rig has been designed so that the only significant loss mechanisms contributing to the deceleration of the rotor are expected to be from the magnetic bearings. The two electric motors will drive the rotor up to top speed at which point the motors will be shut off and the motor stators will be mechanically removed from the motor rotors as shown in the conceptual sketch in Figure 3.

The purpose of the removal of the motor stators is to eliminate any possible effects due to residual magnetism in the motors. Also, by using a motor on each end of the shaft the radial magnetic bearings are loaded equally. There are no thrust bearings and axial centering will be achieved through the reluctance centering effects of the radial magnetic bearings. Therefore the power loss in a vacuum due only to the magnetic bearings can be expressed as:

$$P_k = J\omega\frac{d\omega}{dt} = P_{ha} + P_{hr} + P_e \qquad (7)$$

Since the hysteresis terms vary linearly with speed and the eddy current term varies quadratically with speed Equation (7) can be written as

$$J\omega\frac{d\omega}{dt} = C_{ha}\omega + C_{hr}\omega + C_e\omega^2 \qquad (8)$$

where the C_{ha} and C_{hr} represent alternating and rotational hysteresis coefficients, respectively, and C_e represents the eddy current coefficient. These coefficients are independent of speed and time [6,7,8]. Dividing through by $J\omega$ results in

$$\frac{d\omega}{dt} = \frac{(C_{ha} + C_{hr})}{J} + \frac{C_e\omega}{J} \qquad (9)$$

The intercept of the slope of the rundown curve at low speed is the combination of the hysteresis loss coefficients, C_{ha} and C_{hr}. While the eddy current term deviates from the speed squared model at high speeds this will allow for the separation of eddy current losses from the hysteresis components and thus enable the quantification of the eddy current term.

Figure 4 shows an assembly drawing of the test rotor consisting of a stainless steel shaft with a motor rotor on each end and two magnetic bearing journals mounted inboard of the motors.

The outer diameter of the bearing journals is 89.0 mm (3.5 in) and the test rig is designed to operate up to 50,000 RPM resulting in DN of about 4.5×10^6. The rotor has been designed to operate below the first rotor

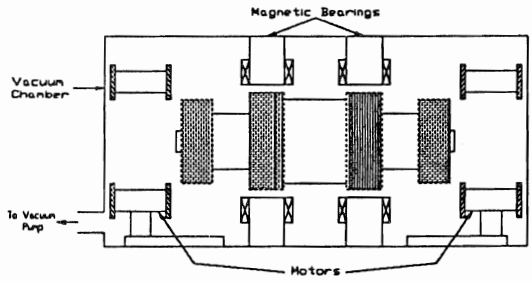

FIGURE 3: Test Set-up: Rundown

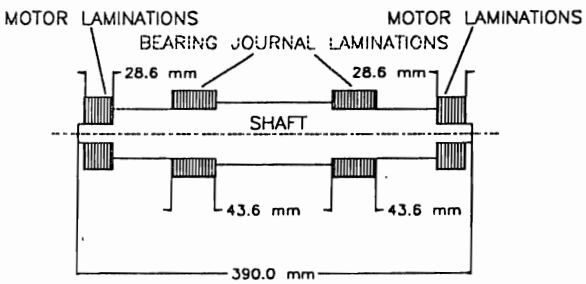

FIGURE 4: Rotor Assembly Drawing

bending mode (located at about 84,000 rpm) so that no bending critical speeds are present in the operating range of interest. An assembly drawing of the entire test rig is shown in Figure 5.

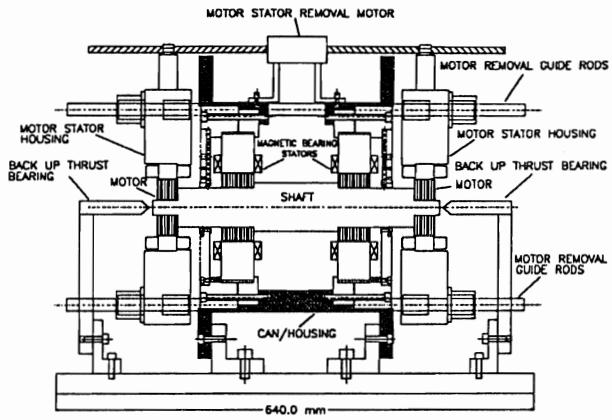

FIGURE 5: Test Rig Assembly Drawing

The housing consists of a can arrangement for mounting bearing stators, back-up bearings and various instrumentation. The "stack-up" design in the can allows for the quick change of components while insuring good alignment. The large blocks located on each outboard end of the can in Figure 5 are the motor stator housings which are mounted on four guide rods to insure accurate linear motion during the motor removal procedure. The housings are attached to nuts mounted on a left hand and a right hand lead screw, respectively, and the lead screws are driven by an electric motor resulting in the linear removal of the motor stators outboard from the motor rotors.

A vacuum chamber encloses the entire test set-up that is shown in Figure 5. Deceleration tests can therefore be run at pressures ranging from atmospheric down to about 10^{-3} mm Hg. The pressure inside the vacuum chamber will be varied to validate the analytical windage model.

While the primary measure of power loss will be the run down time, temperature measurements will also be taken to correlate power losses and subsequent temperature rises. Thermocouples will be attached to bearing stators while non-contacting infrared sensors will monitor the temperature of the journal laminations. Bias and control currents in the bearings will be monitored throughout the rundown for input into the analytical models.

In an effort to separate and quantify individual losses three stator geometries will be analyzed initially including an 8-pole radial planar (heteropolar) bearing, a 16-pole radial planar bearing, and a 2-plane, 8-pole homopolar bearing (without a permanent magnet bias) as shown in Figure 6.

All three of these bearings have equal surface area under the poles, the same tip clearance ratio, and same bias flux to insure comparable bearings except for the

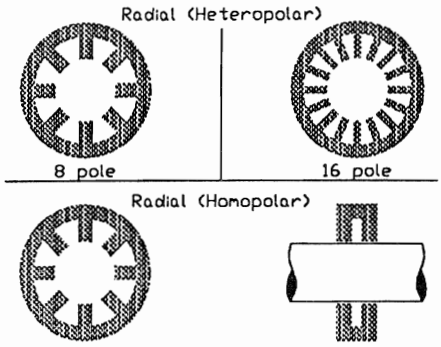

FIGURE 6: Stator Geometries

desired parameter variation. The tip clearance ratio is defined as the ratio between the tip-to-tip chord length and the radial air gap length. The significance of keeping this ratio fixed is to keep an identical shape to the flux field as seen by the rotor for the various bearing configurations. It is expected that the shape of the flux field, dictated by leakage and fringing effects, will affect the magnitude of the losses and will be addressed in this study though not presented here. There is currently significant controversy over claims that the homopolar bearing has lower losses than an equivalent planar bearing.

Because of its common use in existing magnetic bearings, 3% silicon-iron in both a 0.356 mm (0.014in) lamination thickness and a 0.178 mm (0.007in) lamination thickness will be used for the first series of runs. A 0.356 mm (0.014in) lamination thickness was used due to the worldwide unavailability of small quantities of high quality non-oriented silicon iron laminations in a smaller thickness at the time the bearing order was placed. A small reserve of high quality 0.178 mm (0.007in) thick lamination sheet in stock at the University of Virginia enabled the manufacture of a set of journals for the test rotor.

The bias flux is expected to be the primary flux contributor to the losses. Also, because of the static load supported by a radial bearing on a horizontal rotor there is a higher flux level on the upper poles than on the lower poles. The effect of this variation around the rotor will be addressed in future tests possibly by running identical rotors of various weights. Until this effect is quantified, an average bias flux value will be used in the analytical predictions as was done for the low speed tests [5].

Expected run-down times of the rotor from 34,000 RPM for the different configurations where calculated based on analytical expressions developed in [5] and are listed in Table 1. For this series of tests the yield strength of silicon-iron limits the top speed of the rotor to 34,000 rpm, corresponding to a DN of 3.0×10^6. Each journal is expected to see a temperature rise of approximately 60°F assuming there is no conduction or convection of heat.

TABLE 1: Expected Run-Down Times (min)

8-Pole Planar/8-Pole Homopolar	0.178mm Laminations		0.356mm Laminations	
	Vacuum	Air	Vacuum	Air
Bias Flux = 0.25T	27.5	10.0	8.2	5.4
Bias Flux = 0.50T	8.3	5.4	2.3	2.0

16-Pole Planar	0.178mm Laminations		0.356mm Laminations	
	Vacuum	Air	Vacuum	Air
Bias Flux = 0.25T	15.7	7.9	4.3	3.4
Bias Flux = 0.50T	4.5	3.5	1.2	1.1

SENSITIVITY ANALYSIS OF ANALYTICAL EXPRESSIONS

A closer examination of the loss components indicates that the eddy current and windage effects are the major contributors at high speeds. As discussed earlier, the power loss has been determined from low speed tests to consist of four components: alternating hysteresis, rotating hysteresis, eddy current and windage effects [5]. Shown in Figure 7 is a breakdown of the total predicted loss into these four components as obtained from the application of Equations (1-4) for one of the low speed tests [5].

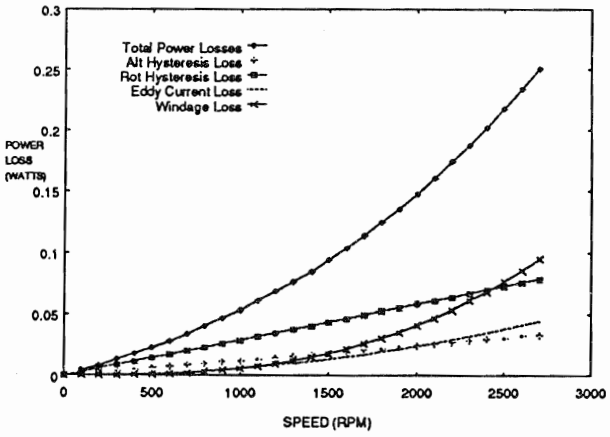

FIGURE 7: Calculated Power Loss Components vs. Speed,Ib=1.6, Paired Poles

While the two hysteresis components dictate the losses at the lower speeds these components increase linearly with speed and are eventually overtaken by the combination of the windage and eddy current losses. The latter increases quadratically with frequency, as per Equation (3). The windage loss increases at an almost cubic rate based on Equation (4). Applying Equations (1-4) (except for the diameter (D) and rotational speed (N)) to one of the high speed test rotor configurations yields:

$$P_e \approx 1.45\text{E-}5\, D^2 N^2$$
$$P_{ha} \approx .019\, D^2 N \qquad (10)$$
$$P_{hr} \approx .023\, D^2 N$$

Therefore, for any diameter, D:

$$P_e \approx P_{ha} + P_{hr} \text{ for } N \approx 3000 \text{ rpm} \qquad (11)$$

Including windage losses,

$$P_w \approx 1.47\text{E-}7\, D^{3.6} N^{2.8} \qquad (12)$$

Now,

$$P_e + P_w \approx P_{ha} + P_{hr} \text{ for } N < 1000 \text{ rpm} \qquad (13)$$

Thus the windage and eddy current effects begin to dominate above rather low speeds for any given diameter. At some frequency the loss due to the eddy current phenomena will begin to fall below the speed squared law due to the crowding effect associated with the eddy currents, thus increasing the relative contribution of the hysteresis components. The point at which this occurs is not well known and will be addressed as tests are underway. The separation of losses as shown in Equations (7)-(9) will isolate the eddy current component in the vacuum environment.

We will limit ourselves here to the characterization of the expected major components (eddy current effects and windage) of the total power loss. The eddy current loss equation expanded from Equation 3 and including a term to account for crowding effects is [10]:

$$P_e = \frac{\pi^3 \mu_o^2 N^2 (M_e f)^2 \tau^2 i_b^2 M_v L D^2}{24 \rho g^2} \left(1 - \left(\frac{6}{945}\right)\left(\pi\tau\sqrt{\frac{2\mu(M_e f)}{\rho}}\right)^4\right) \qquad (14)$$

The value of most of the parameters in this equation for any given bearing are well known within a few percent error except for the eddy current frequency factor, M_e and the effective volume factor, M_v. The eddy current frequency factor (M_e) represents the pertinent frequency component(s) due largely to edge effects and is the most important parameter to quantify. This will be done by measuring power losses in radial planar bearings with 8 and 16 poles, respectively, as well as, in an 8 pole homopolar bearing as shown in Figure 6. Various geometrical characteristics were held constant to insure consistency of the shape of the flux field which is dictated by leakage and fringing in order to isolate the effect of the number of poles. Future tests will examine the effect of various flux field shapes on the loss components by varying tip clearance ratios and possibly by examining variations in pole edge profiles.

The next parameter with the largest uncertainty is the effective volume factor (M_v). This parameter is the percentage of the total journal lamination volume that actively participates in the loss mechanism. In other words, not all of the journal lamination volume

contains the maximum amount of flux and therefore there is some effective volume (which is less than the total volume) which dictates the magnitude of the losses. Preliminary static finite element analysis has characterized this effective volume to some extent [5] but more analysis coordinated with experimental data is necessary for a more accurate determination of the effective volume for various bearing configurations.

The other major loss contributor is windage. Rearranging Equation 4, the windage loss is expressed as:

$$P_W = (3.7E-2)\pi^4 M_W \rho_g L D^{3.6} f^{2.8} \left[\frac{\upsilon}{\pi^2}\right]^2 \qquad (15)$$

Most parameters in this equation are fairly well-known for a given bearing except for the windage loss pole factor (M_W) which represents the effect of poles on the windage loss. This is the most important parameter to quantify. This will be done by measuring power losses in bearings with different numbers of poles and clearances both in air and in vacuums of various magnitudes to verify the analytical models. The windage model could be different for laminar and turbulent flow regimes. Both regimes will be studied by the variation of pressure in the vacuum chamber.

While tests will be run varying other parameters including materials, tip clearance ratio, and lamination thickness, the first series of tests are concerned with characterizing the important frequency components dictating the eddy current losses and the effect of poles in the boundary layer over the journal rotors.

CONCLUSIONS

There are four components of the total power loss in magnetic bearings: alternating hysteresis, rotating hysteresis, eddy current, and windage. At high speeds the eddy current and windage components are expected to dominate. The sensitivity analyses of the analytical expressions for these two components indicate that there are three important parameters to quantify. These are the frequency components which dictate the contribution of the eddy current effects, the effective volume of the rotor where the magnetic flux is entrained, and the effect of the poles on the windage. The eddy current frequency components, expected to be dictated by edge effects, will be characterized by comparing the losses of 8 and 16 pole radial planar bearings and an 8 pole homopolar bearing, all with equal bias flux, identical tip clearance ratios and pole surface area. The effective volume will be determined by comparing finite element models with experimental data. The effect of bearing poles on the windage will also be characterized by comparing data from the two heteropolar bearings and the homopolar bearing and by comparing run-down data taken at different levels of pressure in the vacuum chamber, from atmospheric pressure down to about 10^{-3} mm Hg. It is hoped that the interaction between the analysis of the theory and the experimental data will ultimately forge a comprehensive understanding and characterization of the loss mechanisms in the various operating regimes of magnetic bearings.

ACKNOWLEDGMENTS

This research was funded in part by NASA Lewis Research Center and the Commonwealth of Virginia's Center for Innovative Technology.

REFERENCES

1. Yoshimoto, T., "Eddy Current Effect in Magnetic Bearing Model," IEEE Transactions on Magnetics, Vol. MAG-19, No. 5, Sept. 1983.

2. Matsumura, F., and Hatake, K., "Relation between Magnetic Pole Arrangement and Magnetic Loss in Magnetic Bearing," Proc. of Third Intl. Symp. on Magnetic Bearings, July 29-31, 1992, Alexandria, VA, USA, pp. 274-283.

3. Higuchi, T., Mizuno, T., and Miyake, S., "Experimental Study of Rotational Loss in Magnetic Bearings," Proc. Conf. IPE, Japan, Spring 1986, pp. 53-54.

4. Ueyama, H., and Fujimoto, Y., " Iron Losses and Windy Losses of Rotational Speed Rotor Suspended by Magnetic Bearings," Proc. of 2nd Intl. Symp. on Magnetic Bearings, July 12-14, 1990, Tokyo, Japan, pp. 237-242

5. Kasarda, M., Allaire, P., Humphris, R., and Hope, R., "Comparison of Experimentally Measured and Calculated Losses in Planar Radial Magnetic Bearings," ROCON Conference Proc., Nov 1993.

6. Knowlton, Archer E., Editor-in-Chief, Standard Handbook for Electrical Engineers, McGraw-Hill Book Company, Inc. 1949.

7. Brailsford, F., "Rotational Hysteresis Loss in Electrical Shaft Steels," IEEJ, 1938, pp. 566-575.

8. Matsch,L., Electromagnetic and Electromechanical Machines, Crowell Publishers, 1972.

9. Shames, Irving H., Mechanics of Fluids, McGraw-Hill Book Company, 1982.

10. MIT Electrical Engineering Staff, Magnetic Circuits and Transformers, Wiley, 1943.